

# Optimized analysis method for indirect dark matter searches with Imaging Air Cherenkov Telescopes

J. Aleksić,<sup>a</sup> J. Rico<sup>b,a</sup> and M. Martínez<sup>a</sup>

<sup>a</sup>Institut de Física d'Altes Energies (IFAE),  
Campus UAB, E-08193 Bellaterra, Spain

<sup>b</sup>Institució Catalana de Recerca i Estudis Avançats (ICREA),  
E-08010 Barcelona, Spain

E-mail: [jelena@ifae.es](mailto:jelena@ifae.es), [jrico@ifae.es](mailto:jrico@ifae.es), [martinez@ifae.es](mailto:martinez@ifae.es)

**Abstract.** We propose a dedicated analysis approach for indirect Dark Matter searches with Imaging Air Cherenkov Telescopes. By using the full likelihood analysis, we take complete advantage of the distinct features expected in the gamma ray spectrum of Dark Matter origin, achieving better sensitivity with respect to the standard analysis chains. We describe the method and characterize its general performance. We also compare its sensitivity with that of the current standards for several Dark Matter annihilation models, obtaining gains of up to factors of order of 10. We compute the improved limits that can be reached using this new approach, taking as an example existing estimates for several benchmark models as well as the recent results from VERITAS on observations of the dwarf spheroidal galaxy Segue 1. Furthermore, we estimate the sensitivity of Cherenkov Telescopes for monochromatic line signals. Predictions are made on improvement that can be achieved for MAGIC and CTA. Lastly, we discuss how this method can be applied in a global, sensitivity-optimized indirect Dark Matter search that combines the results of all Cherenkov observatories of the present generation.

**Keywords:** full likelihood, dark matter, indirect searches, Imaging Air Cherenkov Telescopes

---

## Contents

<b>1</b>	<b>Introduction</b>	<b>1</b>
<b>2</b>	<b>Full likelihood method</b>	<b>2</b>
<b>3</b>	<b>Characterization of the full likelihood method</b>	<b>5</b>
3.1	The setup	5
3.2	Optimization of the integration range	7
3.3	Improvement Factor for different signal models	8
3.4	Stability and robustness	10
<b>4</b>	<b>Sensitivity of the full likelihood method for Dark Matter searches</b>	<b>12</b>
4.1	Benchmark models	13
4.2	Secondary gamma rays from annihilation into SM particles	14
4.3	Annihilation into $\gamma\gamma$	16
<b>5</b>	<b>Discussion</b>	<b>17</b>

---

## 1 Introduction

The existence of Dark Matter (DM) has been confirmed by observational evidence on all scales, yet its nature still remains a mystery (for a review, see e.g. [1]). Among theories that try to describe DM and incorporate its presence in our image of the Universe today, the Cold Dark Matter paradigm offers the most satisfactory explanation. It requires the DM particle to be cold, neutral, stable on cosmological scales, consistent with the Big Bang nucleosynthesis and not excluded by the existing experimental constraints [2].

Among the possible candidates complying with these conditions, the Weakly Interacting Massive Particles (WIMPs) are the most widely considered. However, such particles do not exist within the framework of the Standard Model (SM), so one must go beyond its limits to look for WIMPs. For example, the Supersymmetric extension of the SM [3] suggests various natural DM particle candidates, with lightest neutralino being the most studied one. Assuming that neutralinos can self-annihilate, the resulting by-products are expected to be SM particles detectable from Earth, like electrons, positrons, photons and neutrinos.

According to various models (see, e.g., [4]), the DM particle mass is expected to be in the few GeV - few TeV energy range; therefore, highly energetic photons resulting from WIMP annihilation might be visible to the Imaging Air Cherenkov Telescopes (IACTs). Gamma rays are especially attractive from the point of view of indirect DM searches: not only do they trace back to the place of their creation and can be detected from space and ground, their energy pattern also preserves information on the DM particle they originated from. Spectral features like cut-off [5], monochromatic line [6] or spectral hardening due to the internal bremsstrahlung [7] cannot be imitated by the conventional astrophysical sources; as such, they are considered to be the 'smoking guns' of DM detection.

Cherenkov Telescopes have limited duty cycles and great variety of scientific objectives competing for the observation time. Their physics programs are primarily focused on detection and study of astrophysical sources, with fundamental physics and cosmological issues

frequently left on the sidelines. As a consequence, standard analysis tools and methods used to process the observed data are usually optimized for sources with, in the majority of cases, featureless spectral distributions well described by a simple power law.

Such analysis is suboptimal for DM searches, therefore, we propose an improved, dedicated approach of optimized sensitivity for spectral features of DM origin. In comparison with some previous works, that addressed the issue by focusing only on the regions of the spectrum with the most peculiar, DM-induced features (see, e.g. [8] and references within), the method we are suggesting takes full profit of all spectral differences between the signal and the background.

We describe the proposed approach in detail in section 2 and then go on to characterize it and compare its performance with respect to that of the standard IACT analysis in section 3. In section 4, we apply the new method to several models of DM emission, show the improvement achievable with respect to the recently published experimental searches and make observability predictions for different annihilation channels and instruments. Lastly, section 5 is reserved for the discussion and concluding remarks.

## 2 Full likelihood method

In the standard analysis chain of IACTs, the existence of a source is established by a mere comparison of the integrated number of events detected in the source region ( $n$ ) with the number of events detected from the control, background region(s) ( $m$ ). Both  $n$  and  $m$  are random variables that obey Poisson statistics; therefore, the number of gamma-ray ( $g$ ) and background ( $b$ ) events present in the source region can be estimated by maximization of the following likelihood function [9]:

$$\mathcal{L}(g, b|n, m) = \frac{(g+b)^n}{n!} e^{-(g+b)} \times \frac{(\tau b)^m}{m!} e^{-\tau b}, \quad (2.1)$$

where  $\tau$  is the normalisation between the signal and background regions (e.g. ratio of their associated observation times). This, Poisson likelihood to which we also refer as the “*conventional*” likelihood approach, is what is currently used in the standard analysis of the IACT data. Whilst acceptable for sources of astrophysical origin, this method does not make any distinction of the potential features present in the gamma-ray spectrum, and as such, it is suboptimal for the DM searches.

We propose the use of an alternative, more DM-oriented approach: by making an a priori assumption on the expected spectral shape (which is fixed and known for a given DM model), and including it in the maximum likelihood analysis, we can completely exploit the spectral information of the events from DM annihilation and achieve better sensitivity with respect to the conventional method. This *full likelihood* function has, for a given DM model  $M$  with parameters  $\theta$ , the following form:

$$\mathcal{L}(N_{EST}, M(\theta)|N_{OBS}, E_1, \dots, E_{N_{OBS}}) = \frac{N_{EST}^{N_{OBS}}}{N_{OBS}!} e^{-N_{EST}} \times \prod_{i=1}^{N_{OBS}} \mathcal{P}(E_i; M(\theta)), \quad (2.2)$$

with  $N_{OBS}(=n+m)$  and  $N_{EST}$  denoting the total number of observed and estimated events, respectively, in source and background regions.

$\mathcal{P}(E_i; M(\theta))$  is the value of the probability density function (PDF) of the event  $i$  with *measured* energy  $E_i$ . In general,  $\mathcal{P}$  may also depend on the measured arrival time and

direction of the photon, which would reflect on the sensitivity to gamma rays with distinct temporal and spatial structures, respectively. However, signals from DM annihilation are expected to be steady, allowing us to integrate out the time in our analysis. As for the spatial signatures, they may have a more important role for, e.g., galaxy clusters [10], as they can be predicted from halo simulations, although, usually with great uncertainties (see, for example, [11–13]). However, in this work we concentrate mainly on source-candidates that are of angular size smaller or comparable to the typical angular resolution of the IACTs ( $\sim 0.1^\circ$ ) - hence, we do not expect a contribution from a likelihood function dependent on the direction, and we integrate it out as well. Therefore, we define the PDF as a function of measured energy only:

$$\mathcal{P}(E; M(\boldsymbol{\theta})) = \frac{P(E; M(\boldsymbol{\theta}))}{\int_{E_{min}}^{E_{max}} P(E; M(\boldsymbol{\theta})) dE}, \quad (2.3)$$

where  $E_{min}$  and  $E_{max}$  are the lower and upper limits of the considered energy range;  $P(E; M(\boldsymbol{\theta}))$  represents the differential rate of signal and background events, such that:

$$P(E; M(\boldsymbol{\theta})) = \begin{cases} P_B(E_i), & i \in B \\ P_S(E_i; M(\boldsymbol{\theta})), & i \in S \end{cases}, \quad (2.4)$$

with  $P_B(E)$  and  $P_S(E; M(\boldsymbol{\theta}))$  being the expected differential rates from the background ( $B$ ) and source ( $S$ ) regions, respectively:

$$P_B(E) = \tau \int_0^\infty \frac{d\Phi_B}{dE'} R_B(E; E') dE' \quad (2.5)$$

and

$$P_S(E; M(\boldsymbol{\theta})) = \int_0^\infty \frac{d\Phi_B}{dE'} R_B(E; E') dE' + \int_0^\infty \frac{d\Phi_G(M(\boldsymbol{\theta}))}{dE'} R_G(E; E') dE'. \quad (2.6)$$

True energy is denoted with  $E'$ ;  $d\Phi_B/dE'$  and  $d\Phi_G/dE'$  are the differential fluxes of cosmic (background) and gamma-ray (signal) radiations, and  $R_B(E; E')$  and  $R_G(E; E')$  are the telescope response functions to each of them.  $d\Phi_G/dE'$  contains the dependencies on the model parameters ( $\boldsymbol{\theta}$ ).

However, in practice,  $R_B$  can be different for source and background regions, due to its dependence on the direction of the incoming particles within the observed field of view. Such discrepancies are measurable by the telescopes with relatively high precision, and the residual statistical and systematic uncertainties can be taken into account in the likelihood function through inclusion of the relevant nuisance parameters (see, e.g. [9, 14]). In this work we consider that  $R_B$  is equal in eq.(2.5) and eq.(2.6) and known with perfect precision. Nevertheless, in section 3.4 we evaluate the impact its uncertainties may have on our results.

Apart from the shape of the signal spectral distribution, the given model  $M(\boldsymbol{\theta})$  also predicts the expected number of detected events for a given observation time  $T_{OBS}$ :

$$N_{EST} = T_{OBS} \int_{E_{min}}^{E_{max}} P(E; M(\boldsymbol{\theta})) dE, \quad (2.7)$$

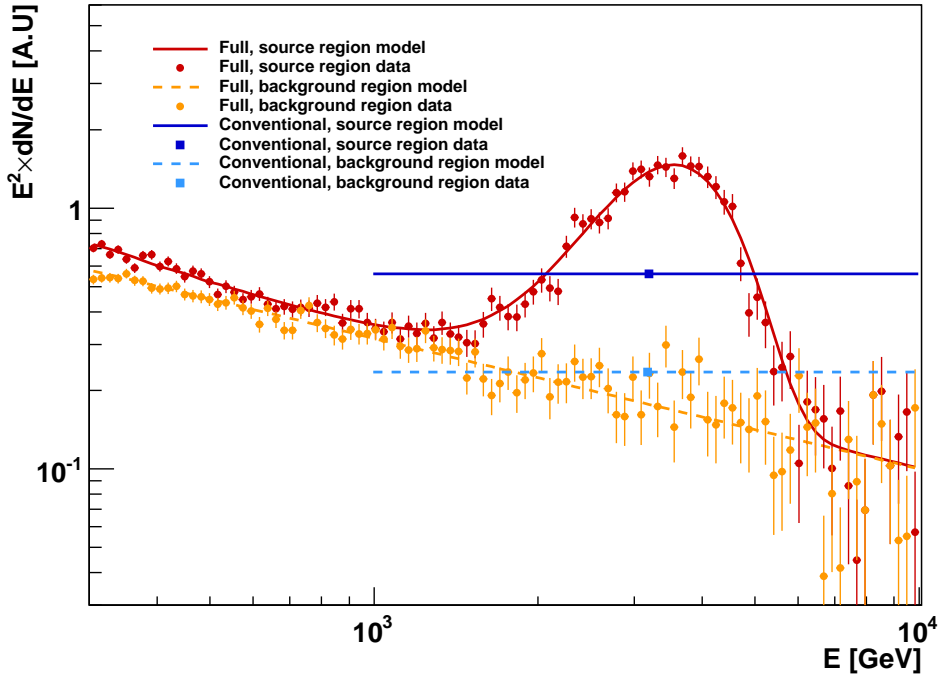


**Figure 1:** Illustration of the advantage of the full likelihood method with respect to the conventional one. Red and orange lines show the assumed spectral energy distributions of the source and background regions, respectively, while the data points, with the same color code, represent the measured events (fine binning is used for demonstration purposes only, the full likelihood is unbinned). The levels of horizontal blue and cyan lines correspond to the average value within the energy range considered in the conventional method, with dots referring to the measurements. See the main text for more details.

included in the full likelihood (eq.(2.2)) through the Poissonian term.

Lastly, for the comparison of the full with conventional analysis, it is worthwhile to note that

$$b = \frac{T_{OBS}}{\tau} \int_{E_{min}}^{E_{max}} P_B(E) dE \quad (2.8)$$

and

$$g(\boldsymbol{\theta}) = T_{OBS} \int_{E_{min}}^{E_{max}} P_S(E; M(\boldsymbol{\theta})) dE - b. \quad (2.9)$$

Figure 1 illustrates the advantage of the full likelihood with respect to the conventional one. Both methods are based on comparisons of the collected data with the predictions from the signal and background models. The conventional method integrates the spectral information in a pre-optimized energy range (for details, see section 3.2), so that the only information used is that of the expected and measured *number of events*. On the other hand, the full likelihood compares the expected and measured *energy distributions*, thus fully profiting from the potential presence of DM spectral features.

### 3 Characterization of the full likelihood method

In this section, in order to evaluate the performance of the full likelihood concept in the IACT analysis, we test it using fast simulations produced under a predefined set of conditions, and compare the results with those of the conventional method obtained under the exact same circumstances.

#### 3.1 The setup

**Response Function.** The response functions  $R_B$  and  $R_G$  of an IACT are governed by its hardware design, reconstruction algorithms, selection criteria for quality of the events and for discrimination between the signal and background. They are computed by means of measurements and full Monte Carlo simulations, and typically can be represented as a product of three factors: effective area  $A_{eff}(E', \hat{p}', t)$ , angular ( $\Sigma(\hat{p}; E', \hat{p}', t)$ ) and energy ( $G(E; E', \hat{p}', t)$ ) reconstruction functions, with  $\hat{p}$  and  $\hat{p}'$  referring to the measured and true directions of the incoming particle, and  $t$  to the time of the detection. As mentioned before, the spatial and temporal dependencies are integrated out in our analysis, so the response functions we use in this work have the form:

$$R_{B,G}(E; E') = A_{eff_{B,G}}(E')G_{B,G}(E; E'). \quad (3.1)$$

The effective area  $A_{eff}$  is the area in which air showers can be observed by the instrument folded with the efficiency of all the cuts applied in the analysis. Cherenkov telescopes are not equally sensitive to gamma and cosmic ray showers, and effective areas for different particles are different as well.

The energy resolution  $\sigma$  is defined as the width of a Gaussian fit to the  $(E - E')/E'$  distribution, while the mean of that fit is the relative energy bias  $\mu$ . However, in the real data analysis, the energy reconstruction function might need to be described by a more accurate parametrization.

For the characterization of the full likelihood method in the following tests, as representative response function of a current-generation IACT, we use the corresponding functions of the MAGIC Telescopes<sup>1</sup> [15].

**Spectral Functions.** The background emission is produced by the cosmic rays, with a flux well described by a simple power law:

$$\frac{d\Phi_B}{dE'} = A_B E'^{-\alpha}, \quad (3.2)$$

with spectral index  $\alpha$  and intensity  $A_B$ . In practice, however, we only need the value of  $P_B(E)$  (eq.(2.5)), which is directly measured by the IACTs (or computed from Monte Carlo simulations for projected instruments).

Regarding the spectral form of the signal emission, at this stage, we consider two simple cases:

(a) power law ( $PL$ ) of spectral index  $\gamma$  and intensity  $A_{PL}$ :

$$\frac{d\Phi_G}{dE'} = A_{PL} E'^{-\gamma}; \quad (3.3)$$

---

<sup>1</sup><http://magic.mppmu.mpg.de>

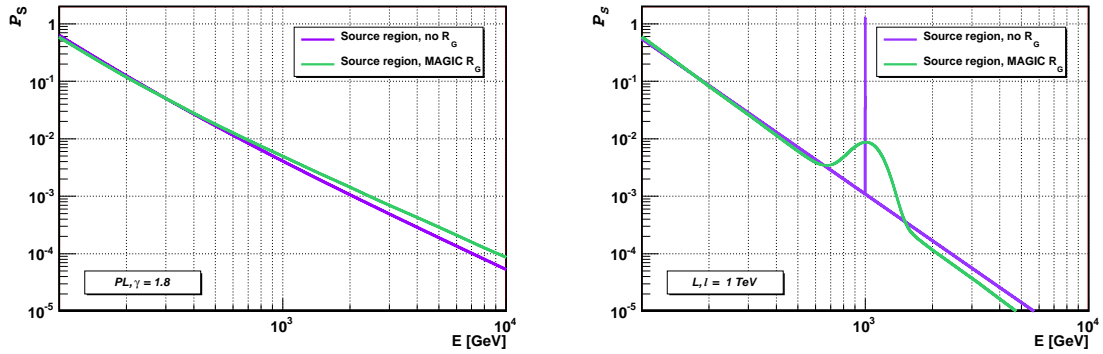


**Figure 2:** Contribution of the source region to the PDF before (purple) and after the convolution (green) with the response function of the telescope. **Left:** The spectral slope of a power law-shaped signal is harder after the convolution. **Right:** A monochromatic line is smoothed and widened due to the finite energy resolution. Shape of the background (**left** and **right**) is also affected by the response function.

(b) a monochromatic line ( $L$ ) at energy  $l$  and of intensity  $A_L$ :

$$\frac{d\Phi_G}{dE'} = A_L \delta(E' - l). \quad (3.4)$$

The convolution of spectral and response functions yields the form of the PDF. As seen in figure 2, the original spectral shape is modified by the imperfect instrument, with features like line being smoothed and hardness of the power law being altered.

**Improvement Factor.** In our tests, we choose the signal intensity ( $A_{PL}$  in the case of a  $PL$ ,  $A_L$  for the line-shaped signal) as a free parameter, whose value is to be estimated by maximization of the likelihood functions (eq.(2.1) and eq.(2.2)). Performance of the full likelihood with respect to the conventional one, for a given signal model  $M(\boldsymbol{\theta})$ , is quantified by means of an *Improvement Factor* ( $IF$ ):

$$IF(M(\boldsymbol{\theta})) = \langle CI_{convn} / CI_{full} \rangle, \quad (3.5)$$

i.e. the average ratio of the widths of the confidence intervals,  $CI_{convn}$  and  $CI_{full}$ , calculated by the corresponding methods, assuming a common confidence level.

The Improvement Factor is, by construction, the *improvement in the sensitivity* of a given search expected by the use of the full likelihood over the conventional approach, provided that both methods produce unbiased estimators. We have explicitly checked this extreme, for several different models of signal emission, without finding any indications for the presence of bias (figure 3).

In this work, the confidence intervals are two-sided and computed following the “ $\ln\mathcal{L} + 1/2$ ” rule and assuming one unconstrained degree of freedom. The maximization of the likelihood functions (eq.(2.1) and eq.(2.2)) is performed using the `TMinuit` class incorporated in the framework of `ROOT` [16, 17]. We have numerically confirmed that the obtained coverages are the expected ones.

For the characterization of the method, the confidence intervals are calculated with 95% confidence level, and their ratio averaged from 25 fast-simulated experiments. Each

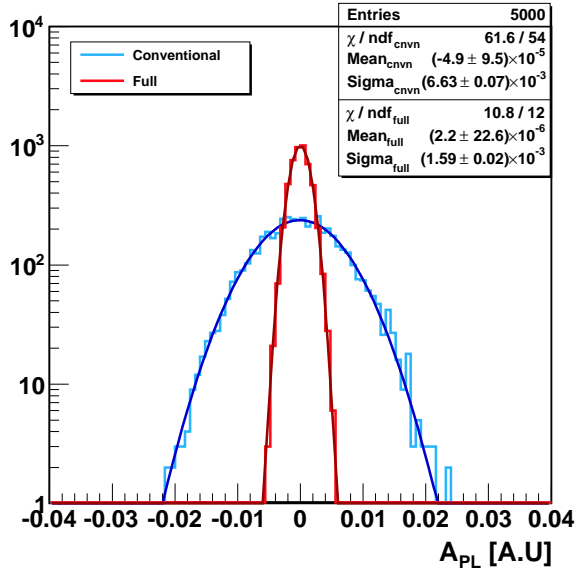


**Figure 3:** Distribution of the free parameter values estimated by the conventional (blue) and full likelihood method (red), for a  $PL$  signal emission model, with  $\gamma = 1.8$ . Test conditions are such that the expected parameter value is zero; results are obtained from 5000 fast-simulated experiments.

simulation consists of  $10^5$  events<sup>2</sup>, randomly generated according to the PDF describing the expected background (i.e. the expected value of the signal intensity is zero), with  $\tau = 2$ ,  $E_{\min} = 100$  GeV and  $E_{\max} = 10$  TeV (unless specified otherwise).

### 3.2 Optimization of the integration range

By definition, the full likelihood takes complete advantage of the signal spectral information, so it makes sense to assume that maximal sensitivity with this method is achieved when the whole energy range is considered. For the conventional concept, however, this does not have to be the case, especially if some distinctive features are expected in the spectra. Here, we study the performance of each method for different energy integration ranges. For a chosen model and a given method, the optimal integration range is the one resulting in the best sensitivity.

In the case of the power law-shaped signal, we fix one integration limit while varying the other: figure 4 shows the mean values of  $CI$ s, calculated with each method, for a signal of  $\gamma = 1.8$  spectral slope and the integration range of fixed  $E_{\min}$  (left) or fixed  $E_{\max}$  (right). As expected, in both cases, the full likelihood is best favoured when the entire energy range is considered. As for the conventional approach, the scenario with fixed  $E_{\max}$  and optimized  $E_{\min}$  yields best sensitivity, and we shall always use such settings in the following tests.

In the case of the spectral line, the sensitivity is optimized by restricting to those events in the vicinity of the peak. Figure 5 shows the  $CI$  widths of the full likelihood and conventional approaches, as a function of the integration range width (expressed in units of  $\sigma$ ), centered at  $l$ . Again, the full likelihood provides best constraints when the complete

<sup>2</sup>The number of events chosen for the characterization, for the selected setup, corresponds to  $\sim 200$  hours of observations. This value depends very much on the chosen instrument and applied analysis cuts (in particular on the energy threshold), but does not have a significant role in the overall Improvement Factor value (for more details, see table 1, section 3.4)



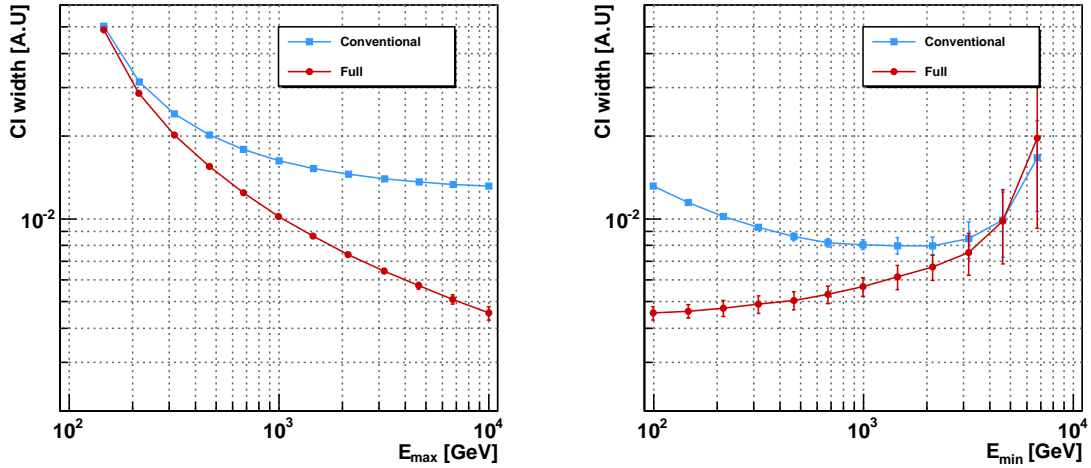


**Figure 4:** Mean widths of the  $CI$ s, calculated with the conventional (blue) and full likelihood (red) methods, as a function of the integration range when  $E_{min}$  (left) or  $E_{max}$  (right) is fixed. The considered signal model is a  $PL$  of spectral slope  $\gamma = 1.8$ . Error bars are the RMS of the  $CI$  distributions.

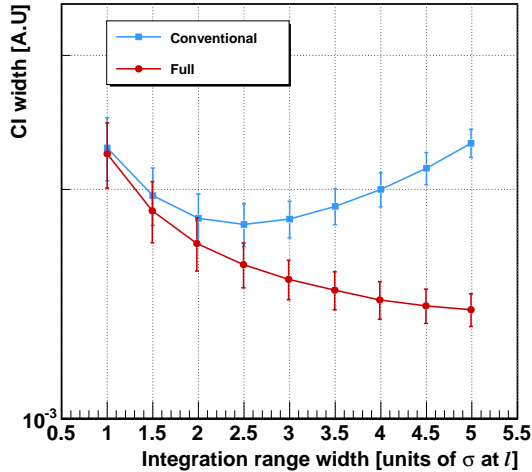


**Figure 5:** Mean widths of the  $CI$ s, calculated with the conventional (blue) and full likelihood (red) methods, as a function of the integration range width given in units of  $\sigma$  around the line energy  $l = 1$  TeV. Error bars are the RMS of the  $CI$  distributions.

energy span is integrated, while the conventional approach is most sensitive for a limited range.

The Improvement Factor values given in the following sections are always calculated from the most constraining upper limits of both methods, using the whole energy range for the full likelihood and the optimized one for the conventional approach.

### 3.3 Improvement Factor for different signal models

In this section we compare the sensitivities of the full likelihood and conventional methods for various  $PL$  and line-shaped signals.

Figure 6a shows the Improvement Factor as a function of the spectral slope  $\gamma$  for  $PL$  models. In this example, for the case when  $\gamma \approx 3.6$ , the shapes of signal and background differential rates are very alike, and therefore the improvement one gains from the use of the

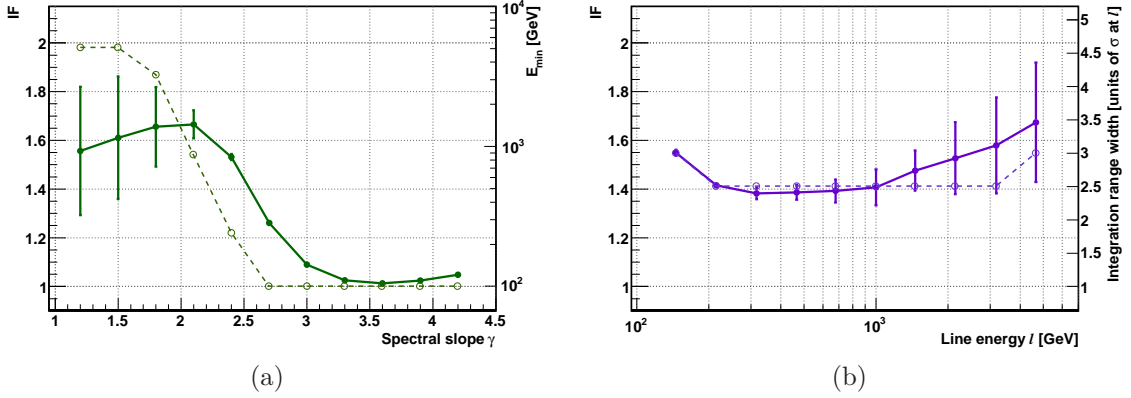


**Figure 6:** Improvement Factor for different  $PL$  (a) and  $L$  (b) signal models (full line). Also shown are the optimal values of  $E_{min}$  and integration range width (conventional approach) for the considered models (dashed line, right-hand axis). Error bars are the RMS of the  $IF$  distributions.

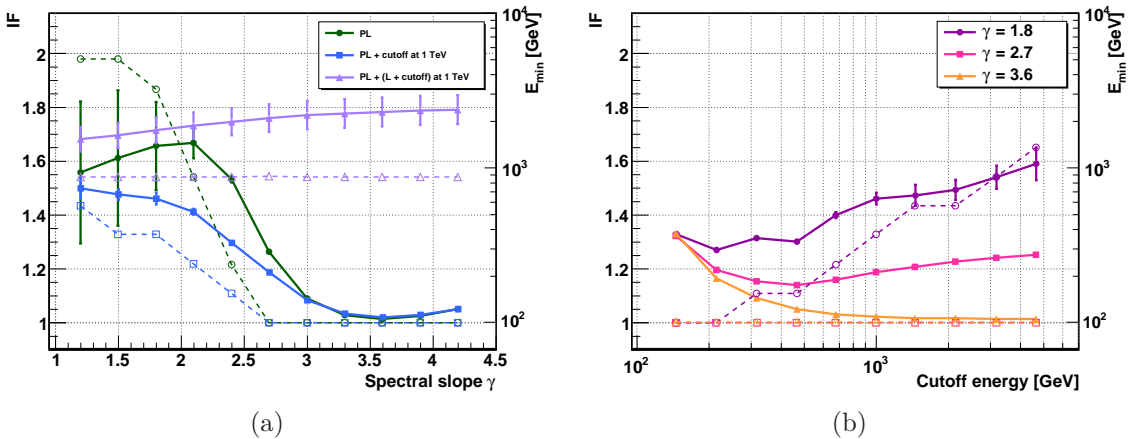


**Figure 7:** Improvement Factor as a function of spectral slope  $\gamma$  (a) and of cutoff energy (b), for different signal models (full lines). Also shown are the optimal values of  $E_{min}$  (conventional approach) for the considered models (dashed lines, right-hand axis). Error bars are the RMS of the  $IF$  distributions.

full likelihood is almost negligible. For harder spectral slopes the improvement on sensitivity of the full with respect to that of the conventional likelihood approach can reach up to 65%. The dashed line indicates the value of  $E_{min}$  for which the conventional method yields the most constraining limit for the given model. For expected signal emissions of harder spectral indices, that dominate over the background radiation at higher energies, the conventional approach is optimized for the upper end of energy region. For increased  $\gamma$ , differences between signal and background concentrate at lower energies, so integration of the full energy range is preferred.

For  $L$  models, depending on the line energy  $l$ , the Improvement Factor can be between  $\sim 40$  and 65% (figure 6b). It is also interesting to note that the width of the optimal integration range (in units of  $\sigma$  at  $l$ ) for the conventional approach is almost constant for all the models and of order of 2.5 - 3.

We can further elaborate the spectral shape of our signal by including additional features of physical interest. For example, the continuous, power law-shaped emission can abruptly cease at a certain energy, resulting in a sharp cutoff in the spectral distribution, smoothed by the response function of the detector. Figure 7a considers the case of  $PL$  models with

different spectral slopes  $\gamma$  that all have a cutoff at a fixed energy of 1 TeV. In the presence of a cutoff, the Improvement Factor is lower than in the case of uninterrupted  $PL$  emission. This is especially noticeable for those signal models that dominate at high energies ( $\gamma < \alpha$ ), since their distinction from the background is partially erased by the cutoff. For the softer spectra, this effect is not that evident, as for those cases signal is more distinguishable from the background at lower energies, i.e. well below the cutoff.

We also inspect how the Improvement Factor depends on the cutoff energy. Figure 7b shows that, for hard spectra, the higher the cutoff, the greater the improvement. For the soft spectra, Improvement Factor is enhanced by low-energy cutoffs to levels comparable to those obtained for spectral lines at similar energies.

Lastly, we study the effect of adding a line to the  $PL$ -with-cutoff spectral distribution. For such models, we take the overall signal intensity as a free parameter, while the individual amplitudes of the  $PL$ ,  $A_{PL}$ , and  $L$ ,  $A_L$ , are set in such a manner that the integrated areas corresponding to those emissions in the PDF are equal. As shown on figure 7a, presence of a line at the same energy as the cutoff ( $l = 1$  TeV) significantly boosts the Improvement Factor value, especially for soft spectra. Its contribution is obvious from the optimal  $E_{min}$  distribution as well: regardless of the value of  $\gamma$ , the most constraining limits from the conventional method are achieved when  $E_{min}$  is just below the line, seeing how this feature is the one dominating the Improvement Factor value.

### 3.4 Stability and robustness

While in the previous subsection we varied the signal model, here we analyse the dependence of the Improvement Factor on the experimental parameters. Table 1 summarizes our results when, for several models of signal emission, we take different values of those parameters that are not affiliated with the DM model itself, but rather with the observational setup ( $\tau$ , number of events), energy resolution of the instrument ( $\sigma$ ) and energy range ( $E_{max}$ ). For the majority of the considered settings, the observed variations of the Improvement Factor value are no more than 1% - 2%, with the following exceptions:

- $\tau$ : the greater the  $\tau$ , the lower the gain provided by the full likelihood method. This is especially noticeable for hard  $PL$  and  $L$  signal models;
- $\sigma$ : in the case of the spectral line, the worse the  $\sigma$ , the greater the improvement. It must be clarified, however, that this does not mean that a poor resolution yields more constraining upper limits, but that the advantage of the full likelihood approach is more significant;
- $E_{max}$ : for the  $PL$  signal models of harder spectra, that dominate over the background at higher energies, the increase of energy range means also the greater Improvement Factor. On the other hand, for softer  $PL$  model, as well as for the considered  $L$ , change of this experimental parameter produces no significant effect.

Additionally, we study the effect the presence of a signal in the data sample may have on the Improvement Factor value. Considering various signal intensities, that yield (for full likelihood) significances of up to 5 standard deviations, we find that the Improvement Factor increases up to  $\sim 10\%$  for signal model of hard power law spectrum, whereas it has no sizable influence for other considered models (table 1).

We also test the robustness of the full likelihood by assuming that the response function of the detector is not precisely known. For this, we simulate events with one response function,

Parameter	Variation Range [units of the parameter]	IF		
		$PL, \gamma = 1.8$	$PL, \gamma = 3.6$	$L, l = 1 \text{ TeV}$
$\tau$	1 - 5	1.91 - 1.47	1.02 - 1.01	1.63 - 1.26
Number of events	$5 \times 10^4 - 5 \times 10^6$	1.66 - 1.62	1.03 - 1.02	1.43 - 1.41
$\sigma$ [% of $\sigma_{MAGIC}$ ]	50 - 500	1.65 - 1.66	1.01 - 1.11	1.37 - 2.83
$E_{max}$ [TeV]	10 - 50	1.65 - 1.82	1.01 - 1.02	1.40 - 1.41
Significance [std. dev]	0 - 5	1.65 - 1.75	1.01 - 1.01	1.40 - 1.42

**Table 1:** Dependence of the Improvement Factor on different experimental parameters for three different representative signal models.

$R_0$ , but use a different one,  $R_W$ , for the likelihood maximization. Data are generated so that they contain a gamma-ray signal of intensity that yields a  $5\sigma$  detection for  $R_0 = R_W$ . We study how the significance of the detection by the full likelihood degrades when  $R_W \neq R_0$ .

First, we consider the effect of using the wrong  $A_{eff}$  function, shifted for a fixed value in energy with respect to the real one. While for  $L$  signal models the sensitivity is not influenced by this discrepancy, for  $PL$ , especially those of soft spectral indices, the sensitivity decreases up to 5% for a 50 GeV shift.

Next, we consider the case of unknown energy resolution  $\sigma$ : for a power law-shaped signal, there is no significant effect - less than 1% decline in sensitivity for a factor 2 mistake in the estimate of  $\sigma$ . On the other hand, in the case of a line, a  $\sigma$  wrong by the same factor leads to a  $\sim 10\%$  worse sensitivity.

Lastly, we assume different energy bias  $\mu$  functions for the simulations and for the likelihood analysis. Our findings show that, for  $\mu$  values shifted from the actual ones by  $1\sigma$  at the given energy, the sensitivity of the analysis decreases  $\sim 5\%$ . If the shift is  $2\sigma$ , the decline is  $\sim 20\%$ . This means that, when searching for a line in the spectrum, we can take as up to  $1\sigma$  wide steps in our scan without risking a significant sensitivity degradation.

Having in mind that even under these extreme and conservative conditions, the worsening in the sensitivity of the full likelihood is still smaller than the improvement one gains from its use (with respect to the conventional approach), we may conclude that this method is robust.

As mentioned in section 2, the background in the source region may be known within some uncertainties. Here we estimate the effect this can have on the results of the conventional and full likelihood methods.

First, we consider energy-dependent differences between the  $R_B$  functions in the source and background regions, parametrized as an extra power law term multiplying the first integral in eq.(2.6). Its index is introduced in the likelihood functions as a nuisance parameter, with a Gaussian probability distribution of mean 0 and width 0.04 (so that maximum deviation of 5% is achieved at any energy). This results in the sensitivity decrease for both the full likelihood and conventional method, but more drastically for the latter one: for the case of the  $L$  models as well as the hard power law-shaped spectra, results from conventional approach are up to  $\sim 50\%$  less constraining. For the full likelihood, the corresponding sensitivity losses are smaller:  $\sim 5\%$  for  $L$  and  $\sim 25\%$  for the  $PL$  signal models. Soft power law spectra are not affected (less than 1%), for either of the analysis methods.

The case of global (normalization) differences is examined by treating  $\tau$  as a nuisance parameter, with a Gaussian probability distribution of a 5% width. This leads to significant sensitivity losses for the conventional method:  $\sim 30\%$  for  $L$  models and  $\sim 10\%$  for hard  $PL$  signals. The full likelihood is again far more robust, exhibiting almost negligible worsening - less than 2% for both kinds of signal models. On the other hand, soft  $PL$  models result problematic for both methods, especially when the spectral shape of the signal is similar to that of the background. The conventional approach suffers from up to a factor  $\sim 8$  worse sensitivity, also for all softer signal models. In the case of the full likelihood this is less pronounced (up to a factor  $\sim 4$  sensitivity worsening), and its power is recovered as soon as the shape of the expected signal becomes different from that of the background. This is caused, for both methods, by high correlation (up to 0.99) between  $\tau$  and signal intensity when the signal and background are of similar spectral shapes. For other signal models the correlation is low, due to the energy range optimization applied in the conventional approach and the presence of the spectral term in the full likelihood.

#### 4 Sensitivity of the full likelihood method for Dark Matter searches

So far we have characterized the performance of the full likelihood in a rather general way, by assuming generic spectral shapes. In this section, however, we explore its sensitivity for specific DM models, for the observations with MAGIC and CTA<sup>3</sup>. The following cases are considered:

- a) benchmark models (BM), as defined by Battaglia et al. (2009) [18] and by Bringmann, Doro and Fornasa (2009) [19]. We compare our results to those presented in [19];
- b) secondary gamma rays from annihilation into SM particles (in particular, we study the  $b\bar{b}$ ,  $\tau^+\tau^-$  and  $W^+W^-$  channels). We also show the sensitivity improvement obtainable through the use of the full likelihood with respect to the recently published VERITAS results of Segue 1 observations [20];
- c) annihilation into  $\gamma\gamma$ . We compare the expected sensitivities to the possible hint of monochromatic line found in Fermi data by Weniger (2012) [21] and more recently by Su and Finkbeiner (2012) [22].

To compute the sensitivity of the full likelihood, we use, in eq.(2.2), the differential gamma-ray flux from the annihilation of DM particles, given as a product of two terms:

$$\frac{d\Phi_G}{dE'} = \frac{d\Phi_G^{PP}}{dE'} \times \tilde{J}(\Delta\Omega). \quad (4.1)$$

The *particle physics* term,  $d\Phi_G^{PP}/dE'$ , describes the characteristics of the chosen DM model:

$$\frac{d\Phi_G^{PP}}{dE'} = \frac{1}{4\pi} \frac{\langle\sigma v\rangle}{2m_\chi^2} \frac{dN_G}{dE'}, \quad (4.2)$$

where  $m_\chi$  refers to the DM particle mass,  $\langle\sigma v\rangle$  is the thermally averaged cross-section, and  $dN_G/dE'$  represents the differential gamma-ray rate per annihilation, summing all possible final states weighted by their corresponding branching ratios.

---

<sup>3</sup><https://www.cta-observatory.org>

The effective *astrophysical factor*,  $\tilde{J}(\Delta\Omega)$ , depends on the distance and morphology of the source, and it is defined as the integral along the line of sight (*los*) of the squared DM density  $\rho$ , integrated over the solid angle  $\Delta\Omega$  of the signal region:

$$\tilde{J}(\Delta\Omega) = \int_{\Delta\Omega} d\Omega \int_{los} \rho^2(r) ds. \quad (4.3)$$

It is reasonable to assume that the  $\tilde{J}$  factor, for a given source and assumed DM distribution profile, is the same for every IACT of the current generation, since their point-spread functions are very alike, and therefore the signal region spans over similar solid angles  $\Delta\Omega$ . Unlike  $\tilde{J}$ ,  $d\Phi_G^{PP}/dE'$  does not depend on the observed source - its value is completely determined for a given theoretical framework.

In the upcoming subsections, we express the sensitivity of the full likelihood approach as the value of  $\langle\sigma v\rangle$  (taken as free parameter in the maximization of the likelihood) for which we would obtain a detection with a given statistical significance in a given  $T_{OBS}$ .

#### 4.1 Benchmark models

Bringmann, Doro and Fornasa (2009) [19] made observability predictions (requiring a  $5\sigma$  detection in 50 hours) for two dwarf Spheroidal galaxies, Draco and Willman 1, for the case of several mSUGRA [23] BM models, and observations with MAGIC and CTA (although, the response functions attributed to each instrument are rather simplified and slightly optimistic). In their calculations, they relied on the conventional likelihood approach, and made two studies: one, for which  $E_{min}$  is the actual energy threshold of the analysis (70 GeV for MAGIC, 30 GeV for CTA), and the other, for which  $E_{min}$  is optimized for each model based on the sensitivity curves of the instruments. In both cases,  $E_{max}$  is selected as the DM particle mass  $m_\chi$ .

We have computed the sensitivities of the full and conventional likelihood approaches under the same circumstances studied in [19]: considering the same DM candidate sources, same BM models of DM emission, and same observatories (but with more realistic response functions: the actual one of MAGIC [15] and one of the latest estimates of the response function of the CTA [24]). The results are shown in table 2, together with the basic characteristics of each of the studied BM models. Improvement Factors  $IF_1$  and  $IF_2$  represent the gain the full likelihood provides over the conventional method, for the two cases of integration ranges considered in [19].

The lowest Improvement Factors (although of values higher than 25%) are obtained, for both MAGIC and CTA, for the practically featureless, soft spectra of the model  $K'$ , as well as for the model  $I'$  from the bulk region, that has a cutoff at low energies. On the other hand, the greatest improvements are achieved in the case of the model  $BM4$ , characterized by the massive DM particle and hard spectrum. Models from coannihilation region, with particularly large internal bremsstrahlung contributions,  $J'$  and  $BM3$ , also show significant gain from the use of the full likelihood (above 60%). Despite these high improvements, however, estimated  $\langle\sigma v\rangle$  limits are still  $\sim 4$  and  $\sim 3$  orders of magnitude, for MAGIC and CTA respectively, away from the predicted values of these BM models.

The fact that our results for  $\langle\sigma v\rangle_{full}$  are about factor  $\sim 2$  less constraining than the conventional limits presented in [19], can be understood by taking into account that the latter were obtained assuming a somewhat idealized situation, with perfectly known background and with flat, optimistic response functions, while we consider circumstances of the real experiment and the actual (or latest from the simulations) responses of the detectors.



BM	$m_\chi$ [GeV]	$\sigma v _{v=0}$ [cm <sup>3</sup> s <sup>-1</sup> ]	MAGIC (>70 GeV)			CTA (>30 GeV)		
			$\langle\sigma v\rangle_{full}$ [cm <sup>3</sup> s <sup>-1</sup> ]	$IF_1$	$IF_2$	$\langle\sigma v\rangle_{full}$ [cm <sup>3</sup> s <sup>-1</sup> ]	$IF_1$	$IF_2$
$I'$	141	$3.6 \times 10^{-27}$	$5.65 \times 10^{-23}$	1.62	1.57	$1.39 \times 10^{-23}$	1.48	1.48
$J'$	316	$3.2 \times 10^{-28}$	$1.01 \times 10^{-23}$	3.64	1.80	$1.91 \times 10^{-24}$	5.18	1.65
$K'$	565	$2.6 \times 10^{-26}$	$3.91 \times 10^{-23}$	1.23	1.23	$8.39 \times 10^{-24}$	1.58	1.58
$BM3$	233	$9.2 \times 10^{-29}$	$7.21 \times 10^{-25}$	4.14	1.89	$1.35 \times 10^{-25}$	6.62	1.61
$BM4$	1926	$2.6 \times 10^{-27}$	$2.87 \times 10^{-23}$	2.10	2.10	$4.82 \times 10^{-24}$	3.81	3.81

**Table 2:** Characteristics of the studied BM models (mass  $m_\chi$  and predicted annihilation cross section today  $\sigma v|_{v=0}$ ), together with the upper limits on the  $\langle\sigma v\rangle$  value calculated with full likelihood method ( $\langle\sigma v\rangle_{full}$ ), for Willman 1 observations with MAGIC and CTA. We also quote the Improvement Factors obtainable from full likelihood with respect to the conventional approach, computed according to the prescription presented in [19]:  $IF_1$  is calculated for an integration range (for the conventional method) from energy threshold to  $m_\chi$ , while for  $IF_2$  the integration is done from optimized lower limit to  $m_\chi$ .

## 4.2 Secondary gamma rays from annihilation into SM particles

One of the most recent results from indirect DM searches with IACTs comes from the VERITAS Collaboration<sup>4</sup>, from observations of the dwarf spheroidal galaxy Segue 1 [20]. Although this source is considered to be one of the most DM dominated objects known so far [25, 26], nearly 50 hours of data showed no significant gamma-ray excess. Consequently, upper limits to the  $\langle\sigma v\rangle$  were derived, for the full energy range and relying on the conventional likelihood analysis.

We have computed how these results could be further strengthened if the full likelihood was used instead. For three final state channels,  $b\bar{b}$ ,  $\tau^+\tau^-$  and  $W^+W^-$  (100% branching ratios), we estimate the limits using both methods and calculate the Improvement Factor values for the upper limits on the DM particle annihilation cross section value  $\langle\sigma v\rangle$ . Following the prescription from [20], we assume  $\tau = 1/0.084$ ,  $T_{OBS} = 47.8$  hours,  $\tilde{J} = 7.7 \times 10^{18}$  GeV<sup>2</sup> cm<sup>-5</sup>, and we calculate the upper limits with 95% confidence level. In the lack of the VERITAS response function used for the analysis in [20], we use the  $A_{eff}$  function from Wood (2010) [27],  $\sigma$  from [28] and we assume a conservative  $\mu = 0$ . The total background rate is taken from [20], approximating the shape of  $P_B$  dependence on energy by that of MAGIC. For the  $dN_G/dE'$  of the studied channels we use the parametrization from Cembranos et al. (2010) [29].

Figure 8a shows our estimates of  $\langle\sigma v\rangle$  limits, calculated by both full and conventional likelihood approaches, assuming observations with VERITAS, for considered channels and following the analysis prescription as given in [20]. The more massive the DM particle, the greater the improvement, especially for the  $\tau^+\tau^-$  channel whose spectra gets harder for higher  $m_\chi$  values. This is partially due to the non-optimization of the integration range in the VERITAS analysis. Gain achievable through the use of the full likelihood is quite significant: for example, the Improvement Factors for  $m_\chi = 100$  GeV, 1 TeV and 10 TeV, are 1.2, 1.6 and 3.4 (for the  $b\bar{b}$  channel), 1.2, 2.9 and 10.1 (for the  $\tau^+\tau^-$ ) and 1.3, 1.5 and 4.5 (for the  $W^+W^-$  channel), respectively. Our estimates do not rely on the actual response function used in [20], and our limits from the conventional likelihood are slightly less constraining than those reported by VERITAS. Nevertheless, we confirm that the consistent Improvement Factor

<sup>4</sup><http://veritas.sao.arizona.edu>

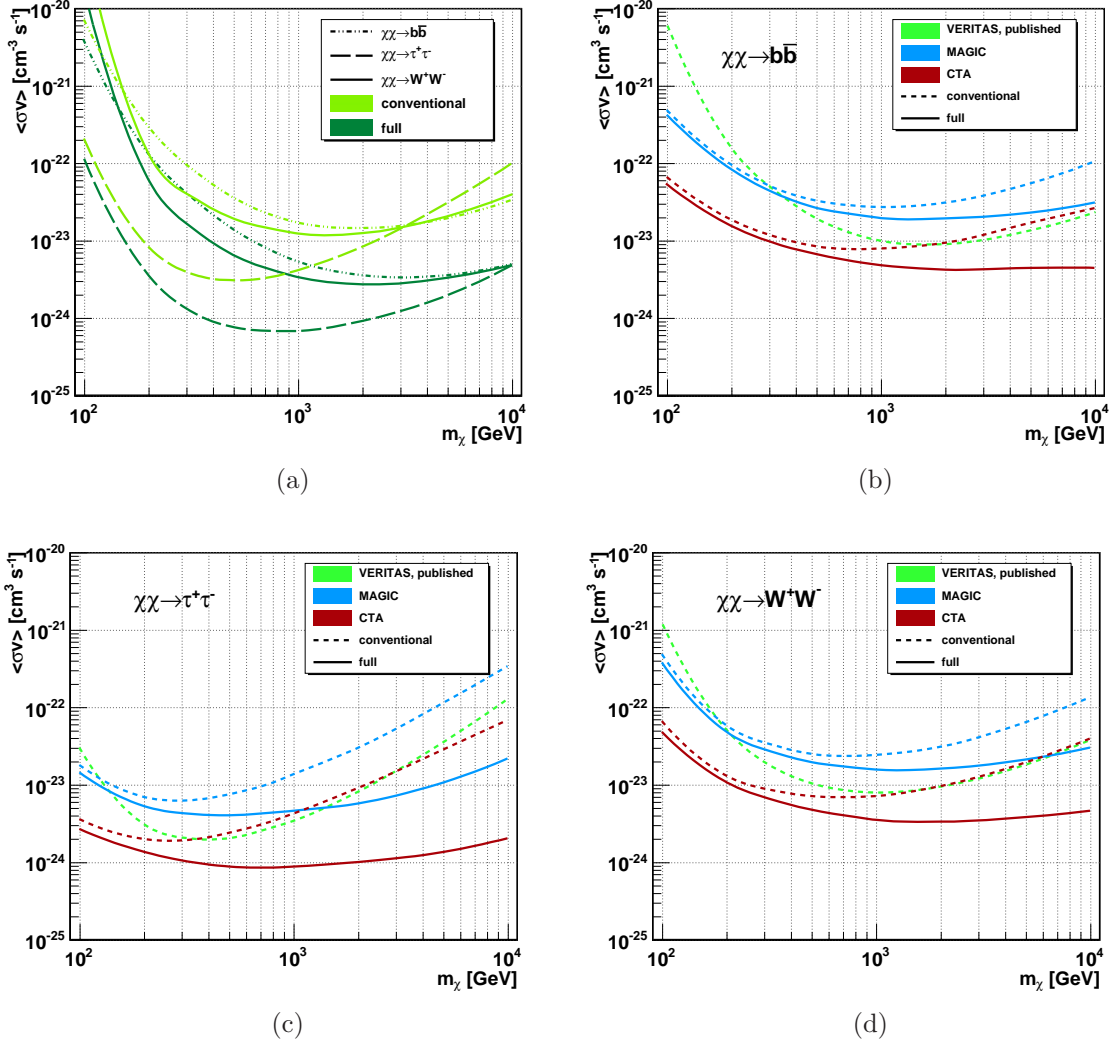


**Figure 8:** 95% confidence level upper limits on the  $\langle\sigma v\rangle$  as a function of  $m_\chi$ , considering different final state particles, and  $\sim 50$  h of observations of the Segue 1 galaxy. (a) Results for VERITAS, from this work, estimated by the conventional (light green) and from the full likelihood approach (dark green). Exclusion lines for (b)  $\chi\chi \rightarrow b\bar{b}$ , (c)  $\chi\chi \rightarrow \tau^+\tau^-$  and (d)  $\chi\chi \rightarrow W^+W^-$  channels, for MAGIC (blue) and CTA (red), obtained from both the conventional (dashed line) and full likelihood approach (full line). (b-d) Results from VERITAS, as given in [20], are also plotted for the comparison purposes (green).

results ( $< 5\%$  difference) are obtained when different  $A_{eff}$  function is used (McCutcheon (2012) [30]). From this, we infer the validity of the obtained Improvement Factor values also for the response function actually applied in the analysis from [20].

Additionally, we study the sensitivities of MAGIC and CTA for the gamma-ray spectra from  $b\bar{b}$ ,  $\tau^+\tau^-$  and  $W^+W^-$  channels, assuming the same observational and analysis conditions as in the case of VERITAS, but using the actual/simulated response functions of these instruments. Exclusion lines, calculated by means of both full likelihood and conventional methods, are shown on figure 8b-8d. As expected, the CTA results are always better than those of MAGIC: at lower energies, by a factor  $\sim 5$ , and by more than one order of magnitude at high energies. Again, the constraints from the full likelihood approach are more significantly improved with respect to the conventional ones for more massive DM particles, and the lowest  $\langle\sigma v\rangle$  limits are achieved for the  $\tau^+\tau^-$  channel (hardest spectrum). For MAGIC,



Improvement Factors for DM particle masses of  $m_\chi = 100$  GeV, 1 TeV and 10 TeV are rather relevant: 1.2, 1.4 and 3.4 ( $b\bar{b}$ ), 1.3, 2.9 and 15.8 ( $\tau^+\tau^-$ ) and 1.3, 1.5 and 4.5 ( $W^+W^-$ ). In the case of CTA, these values are even more significant: 1.3, 1.7 and 6.0 ( $b\bar{b}$  channel), 1.3, 4.8 and 33.1 ( $\tau^+\tau^-$  channel) and 1.4, 2.0 and 8.5 ( $W^+W^-$  channel), respectively.

According to the results shown on figure 8b-8d, the sensitivity gain of the CTA with respect to VERITAS would be marginal, or even nonexistent, for certain annihilation channels and mass ranges. We have traced this inconsistency down to a probable overestimation of the VERITAS performance assumed in [20]. For that, we have used the response functions assumed for VERITAS and those of MAGIC and CTA to compute the integral sensitivity ( $5\sigma$  significance in 50 hours of observations) for a Crab-like spectrum<sup>5</sup> at the analysis threshold<sup>6</sup>, for the different instruments. The results obtained for MAGIC (1.3% of Crab flux above 110 GeV) and CTA (0.30% of Crab flux above 75 GeV) are consistent with those published by the respective Collaborations ([15],[24]). On the other hand, our results for VERITAS, estimated assuming the  $A_{eff}$  from [27], imply a sensitivity of 0.32% of Crab flux above 165 GeV, more than a factor 2 better than the one reported at [31]. And given how the DM constraints reported in [20] are stronger than those computed in this work, we can expect this discrepancy to be even larger for the  $A_{eff}$  actually used in the analysis by the VERITAS Collaboration.

### 4.3 Annihilation into $\gamma\gamma$

Although theoretically highly suppressed, direct annihilation of the DM particles into gamma rays would result in a presence of a sharp line in the energy spectrum, whose detection would represent an unambiguous confirmation of the DM existence.

We have made estimates, using the full likelihood approach, of the sensitivity MAGIC and CTA observatories have to spectral lines, for the DM particle mass in the energy range between 100 GeV and 5 TeV. We require a  $5\sigma$  detection in 50 hours of observations of Segue 1, with Einasto[32] DM profile ( $\tilde{J} = 1.7 \times 10^{19}$  GeV<sup>2</sup> cm<sup>-5</sup> [33]). For the size of the background region we take  $\tau = 12$ . Results are shown on figure 9. MAGIC and CTA exhibit greatest sensitivity for  $m_\chi$  around 200 and 500 GeV, respectively, with CTA being a factor between  $\sim 5$  and  $\sim 10$  better than MAGIC. Furthermore, for the greater part of the considered  $m_\chi$  space, the CTA even slightly probes the  $\langle\sigma v\rangle$  region below the weak-scale cross-section value,  $\sim 3 \times 10^{-26}$  cm<sup>3</sup> s<sup>-1</sup>.

Recent work from Weniger (2012) [21] claims a hint of a gamma-ray line at energy of  $\sim 129$  GeV, from 43 months of Galactic Halo public Fermi data and search restricted to the 20 - 300 GeV range. The inferred value of  $\langle\sigma v\rangle$  is  $1.27 \times 10^{-27}$  cm<sup>3</sup> s<sup>-1</sup> (assuming Einasto profile). As seen from figure 9, neither MAGIC nor CTA are close to reaching that sensitivity using Segue 1 observations.

On the other hand, observations of a source of much higher  $\tilde{J}$  should result in better constraints. For example, 50 hours of CTA observations of the Galactic Halo (assuming NFW density profile,  $\tilde{J} = 3.3 \times 10^{21}$  GeV<sup>2</sup> cm<sup>-5</sup> and  $\tau = 2$ ) would yield order of 30 times better sensitivity than in the case of Segue 1 (figure 9). Furthermore, 50 hours of data would be sufficient for the CTA to test Weniger's claim. It must be noted, however, that this computation does not take into account the systematic uncertainties, which might be relevant for this search (given how the gamma-ray rate would be  $\sim 2\%$  that of the background).

<sup>5</sup> $dN/dE = 5.8 \times 10^{-13} (E/300\text{GeV})^{-2.32-0.13 \log_{10}(E/300\text{GeV})}$  GeV<sup>-1</sup> cm<sup>-2</sup> s<sup>-1</sup> [15]

<sup>6</sup>Defined as the peak of gamma-ray rate true energy distribution

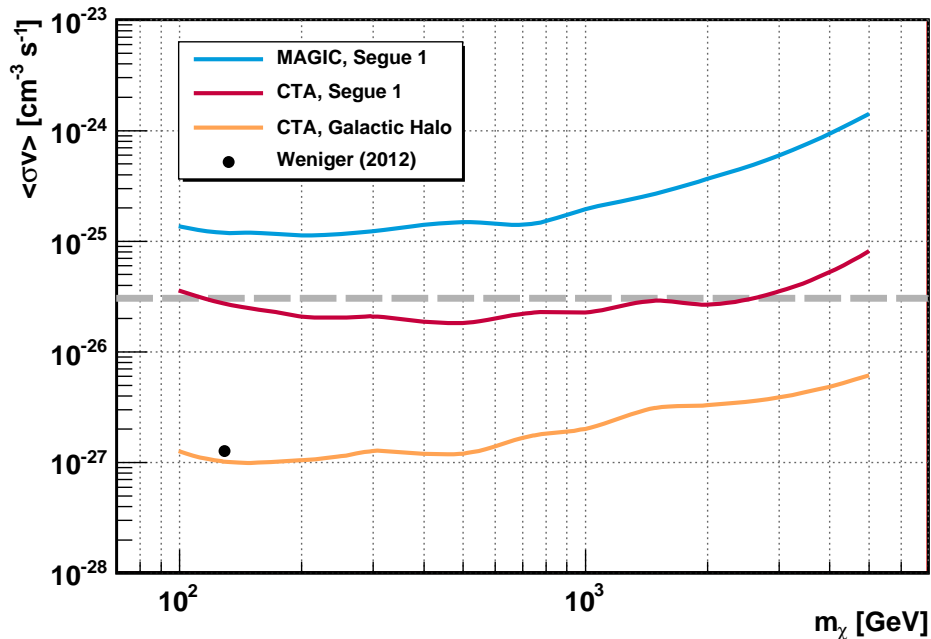


**Figure 9:** MAGIC (blue) and CTA (red) sensitivities on the  $\langle\sigma v\rangle$  values as a function of  $m_\chi$ , for 50 hours of Segue 1 observations, assuming a 100% branching ratio into  $\gamma\gamma$ . Also plotted are the sensitivity predictions for the CTA observations of the Galactic Halo (orange), as well as the  $\langle\sigma v\rangle$  value corresponding to DM signal hint, at  $m_\chi = 129$  GeV, claimed in [21].

## 5 Discussion

We have presented an analysis approach for IACTs that uses the full likelihood method, constructed to take the maximal advantage of the unique spectral features of DM origin. Almost solely through the inclusion of the a priori knowledge on the expected gamma-ray spectrum in the likelihood, this method accedes better sensitivity of the analysis, with Improvement Factors reaching values up to order of 10 (depending on the signal model) with respect to the recent IACT results. In addition, as shown in section 3.4, these improvements are rather insensitive to other analysis characteristics, like the background estimation or signal-to-background discrimination. As a result, the full likelihood can be combined to any other analysis developments aimed at further sensitivity enhancements.

In this work, we have focused on the indirect searches for DM annihilation signals with IACTs. This is reflected in the specific form of the likelihood function (eq.(2.2)), determined by the fact that IACT observations are pointed, cover a relatively narrow field of view, and are dominated by background events. Although, to our knowledge, never used for IACTs, this concept is a well known analysis method, successfully applied in other fields, including DM searches with different techniques and instruments. For instance, a similar approach is employed in the direct detection experiments, like XENON100 [34], and even more extensively, in the indirect searches for DM signals in gamma rays by the Fermi-LAT<sup>7</sup> (see, e.g., [35–37]).

The proposed method is sufficiently general to be used in studies of other physics cases studied by the IACTs, the only condition being that a prediction about the expected spectral

<sup>7</sup><http://fermi.gsfc.nasa.gov>

distribution can be made. A trivial example is the search for DM decay signals, for which we only need to substitute the  $\rho^2$  term by  $\rho$  in eq.(4.3) and  $\langle\sigma v\rangle/2m_\chi^2$  by  $1/\tau_\chi m_\chi$  in eq.(4.2) (with  $\tau_\chi$  referring to the DM particle decay lifetime). Another example where the full likelihood can be successfully applied is in the search of the AGN spectra for signatures induced by the oscillations of gammas into axion-like particles in the presence of intergalactic magnetic fields [38]. This case, however, would require the a priori assumptions on the AGN emission and effects of gamma rays interacting with the extragalactic background light.

Very important characteristic of the full likelihood method (and any likelihood function-based analysis) is that it allows a rather straightforward combination of the results obtained by different instruments and from different targets. For a given DM model  $M(\boldsymbol{\theta})$ , and  $N_{\text{inst}}$  different instruments (or measurements), a global likelihood function can be simply written as:

$$\mathcal{L}_T(M(\boldsymbol{\theta})) = \prod_{i=1}^{N_{\text{inst}}} \mathcal{L}_i(M(\boldsymbol{\theta})). \quad (5.1)$$

This approach eliminates the complexity required for a common treatment of data and response functions of different telescopes or analyses, required by, e.g. the data stacking method (see, e.g. [39]). Within the likelihood scheme, the details of each experiment do not need to be combined or averaged. The only necessary information is the value of the likelihood, expressed as a function of the free parameter (e.g.  $\langle\sigma v\rangle$ ) of a given model for different instruments. Since DM signals are universal and do not depend on the observed target, the results from different sources can also be combined through the overall likelihood function (as done by Fermi [40]), providing therefore a more sensitive DM search. For example, combined results (of similar sensitivities to  $\langle\sigma v\rangle$ ) from three different observatories (e.g. MAGIC, VERITAS and HESS<sup>8</sup>) would benefit from an extra improvement in the sensitivity by a factor of  $\sim 70\%$ . This approach would offer the best chances of discovering DM in indirect VHE gamma-ray searches or of setting the most stringent limits attainable by this kind of observations, placing therefore a new landmark in the field.

**Acknowledgements** Authors wish to give thanks to Michele Doro, Julian Sitarek, Victor Stamatescu and especially to Abelardo Moralejo, for providing some needed data and for very useful discussions. This work has been supported by Spanish MICINN through the programs FPA (grants FPA2009-07474 and FPA2010-22056-C06-01) and Consolider-Ingenio-2010 (grant MultiDark CSD2009-00064).

## References

- [1] G. Bertone, D.Hooper and J. Silk, *Particle Dark Matter: Evidence, candidates and constraints*, *Phys. Rept.* **405** (2005) 279-390 [arXiv:hep-ph/0404175]
- [2] M. Taoso, G. Bertone and A. Masiero, *Dark Matter Candidates: A ten-point test*, *JCAP* **03** (2008) 022 [arXiv:0711.4996]
- [3] J. Wess and B. Zumino, *Supergauge transformations in four dimensions*, *Nucl. Phys.* **B70** (1974) 39
- [4] J. L. Feng, *Dark Matter Candidates from Particle Physics and Methods of Detection*, *Ann.Rev. Astron. Astrophys.* **48** (2010) 495 [arXiv:1003.0904]

---

<sup>8</sup><http://www.mpi-hd.mpg.de/hfm/HESS>

- [5] A. Birkedal, K. T. Matchev, M. Perelstein and A. Spray, *Robust gamma ray signature of WIMP dark matter*, (2005) [[arXiv:hep-ph/0507194](#)]
- [6] L. Bergström and P. Ullio, *Full one-loop calculation of neutralino annihilation into two photons*, *Nucl. Phys.* **B504** (1997) 27-44 [[arXiv:hep-ph/9706232](#)]
- [7] T. Bringmann, L. Bergström and J. Edsjö, *New Gamma-ray Contributions to Supersymmetric Dark Matter Annihilation*, *JHEP* **01** (2008) 049 [[arXiv:0710.3169](#)]
- [8] T. Bringmann et al., *Fermi LAT Search for Internal Bremsstrahlung Signatures from Dark Matter Annihilation*, *JCAP* **07** (2012) 054 [[arXiv:1203.1312](#)]
- [9] W. A. Rolke, A. M. López and J. Conrad, *Limits and confidence intervals in the presence of nuisance parameters*, *Nucl. Instrum. Methods Phys. Res. A*, Vol. **551** (2005) 493-503 [[arXiv:physics/0403059](#)]
- [10] A. Pinzke, C. Pfrommer and L. Bergstrom, *Prospects of detecting gamma-ray emission from galaxy clusters: cosmic rays and dark matter annihilations*, *Phys. Rev. D* **84** (2012) 123509 [[arXiv:1105.3240](#)]
- [11] J. F. Navarro, C. S. Frenk and S. D. White, *The Structure of Cold Dark Matter Halos*, *Astrophys. J.* **462** (1996) 563 [[arXiv:astro-ph/9508025](#)]
- [12] B. Moore et al., *Cold collapse and the core catastrophe*, *Mon. Not. Roy. Astron. Soc.* **310** (1999) [[arXiv:astro-ph/9903164](#)]
- [13] L. Bergström, P. Ullio and J. H. Buckley, *Observability of Gamma Rays from Dark Matter Neutralino Annihilations in the Milky Way Halo*, *Astropart. Phys.* **9** (1998) 137 [[arXiv:astro-ph/9712318](#)]
- [14] H. Dickinson and J. Conrad, *Combined Source Analyses for Atmospheric Cherenkov Telescopes*, (2012) [[arXiv:1203.5643](#)]
- [15] MAGIC Collaboration, J. Aleksić et al., *Performance of the MAGIC stereo system obtained with the Crab Nebula data*, *Astropart. Phys.* **35** (2012) 435-448 [[arXiv:1108.1477](#)]
- [16] F. James, *MINUIT. Function Minimization and Error Analysis, Reference Manual Version 94.1, CERN Program Library Long Writeup D506*, CERN Geneva (1994)
- [17] <http://root.cern.ch/root/html/TMinuit.html>
- [18] M. Battaglia et al., *Updated post-WMAP benchmarks for supersymmetry*, *Eur. Phys. J.* **C33** (2004) 273296 [[arXiv:hep-ph/0306219](#)]
- [19] T. Bringmann, M. Doro, and M. Fornasa, *Dark Matter Signals from Draco and Willman 1: Prospects for MAGIC II and CTA*, *JCAP* **01** (2009) 16 [[arXiv:0809.2269](#)]
- [20] VERITAS Collaboration, E. Aliu et al., *VERITAS Deep Observations of the Dwarf Spheroidal Galaxy Segue 1*, *Phys. Rev. D* **85** (2012) 062001 [[arxiv:1202.2144](#)]
- [21] C. Weniger, *A Tentative Gamma-Ray Line from Dark Matter Annihilation at the Fermi Large Area Telescope*, *JCAP* **08** (2012) 007 [[arXiv:1204.2797](#)]
- [22] M. Su and D. P. Finkbeiner, *Strong Evidence for Gamma-ray Line Emission from the Inner Galaxy*, (2012) [[arXiv:1206.1616](#)]
- [23] H. P. Nilles, *Supersymmetry, Supergravity and Particle Physics*, *Phys. Rep.* **110** (1984) 1-162
- [24] The CTA Consortium, M. Actis et al., *Design concepts for the Cherenkov Telescope Array CTA: an advanced facility for ground-based high-energy gamma-ray astronomy*, *Exp. Astron.* **32** (2011) 193-316 [[arXiv:1008.3703](#)]
- [25] M. Geha et al., *The Least-Luminous Galaxy: Spectroscopy of the Milky Way Satellite Segue 1*, *Astrophys. J.* **692** (2009) 1464-1475 [[arXiv:0809.2781](#)]

- [26] R. Essig et al., *Indirect Dark Matter Detection Limits from the Ultra-Faint milky Way Satellite Segue 1*, *Phys. Rev. D* **82** (2010) 123503 [arXiv:1007.4199]
- [27] M. Wood, 2010. *An Indirect Search for Dark Matter with VERITAS*. Ph.D. University of California
- [28] J. Holder, 2011, *VERITAS: Status and Highlights*, 32nd ICRC, Beijing, China
- [29] J. A. R. Cembranos et al., *Photon spectra from WIMP annihilation*, *Phys. Rev. D* **83** (2011) 083507 [arXiv:1009.4936]
- [30] M. McCutcheon, 2012. *Search for VHE gamma-ray emission from the globular cluster M13 with VERITAS*. Ph.D. McGill University
- [31] <http://veritas.sao.arizona.edu/about-veritas-mainmenu-81/veritas-specifications-mainmenu-111>
- [32] J. F. Navarro et al., *The diversity and similarity of simulated cold dark matter haloes*, *Mon. Not. Roy. Astron. Soc* **402** (2010) 21-34 [arXiv:0810.1522]
- [33] MAGIC Collaboration, J. Aleksić et al., *Searches for Dark Matter Annihilation Signatures in the Segue 1 satellite galaxy with the MAGIC-I Telescope*, *JCAP* **06** (2011) 035 [arXiv:1103.0477]
- [34] XENON100 Collaboration, E. Aprile et al., *Likelihood Approach to the First Dark Matter Results from XENON100*, *Phys. Rev. D* **84** (2011) 052003 [arXiv:1103.0303]
- [35] Fermi-LAT Collaboration, M. Ackermann et al., *Constraints on Dark Matter Annihilation in Clusters of Galaxies with the Fermi Large Area Telescope*, *JCAP* **05** (2010) 025 [arXiv:1002.2239]
- [36] Fermi-LAT Collaboration, A. A. Abdo et al., *Observations of Milky Way Dwarf Spheroidal Galaxies with the Fermi-Large Area Telescope Detector and Constrains on Dark Matter Halo Models*, *Astrophys. J.* **712** (2010) 147-158 [arXiv:1001.4531]
- [37] Fermi-LAT Collaboration, A. A. Abdo et al., *Fermi Large Area Telescope Search for Photon Lines from 30 to 200 GeV and Dark Matter Implications*, *Phys. Rev. Lett.* **104** (2010) 091302 [arXiv:1001.4836]
- [38] M. A. Sanchez-Conde et al., *Hints of the existence of Axion-Like-Particles from the gamma-ray spectra of cosmological sources*, *Phys. Rev. D* **79** (2009) 123511 [arXiv:0905.3270]
- [39] MAGIC Collaboration, J. Aleksić et al., *Gamma-ray excess from a stacked sample of high- and intermediate-frequency peaked blazars observed with the MAGIC telescope*, *Astrophys. J.* **729** (2011) 115 [arXiv:1002.2951]
- [40] Fermi-LAT Collaboration, M. Ackermann et al., *Constraining Dark Matter Models from a Combined Analysis of Milky Way Satellites with Fermi Large Area Telescope*, *Phys. Rev. Lett* **107** (2011) 241302 [arXiv:1108.3546]